LOCAL ENERGY AND PARTICLE TRANSPORT IN BURST-FREE H-PHASES OF ASDEX

G. Becker, ASDEX Team[+] and Neutral Injection Team[++]

IPP III/99

July 1984

MAX-PLANCK-INSTITUT FÜR PLASMAPHYSIK

8046 GARCHING BEI MÜNCHEN

MAX-PLANCK-INSTITUT FÜR PLASMAPHYSIK

GARCHING BEI MÜNCHEN

LOCAL ENERGY AND PARTICLE TRANSPORT IN BURST-FREE H-PHASES OF ASDEX

G. Becker, ASDEX Team[+] and Neutral Injection Team[++]

IPP III/99

July 1984

Die nachstehende Arbeit wurde im Rahmen des Vertrages zwischen dem Max-Planck-Institut für Plasmaphysik und der Europäischen Atomgemeinschaft über die Zusammenarbeit auf dem Gebiete der Plasmaphysik durchgeführt.

IPP III/99 G. Becker, ASDEX Team[+] and Neutral Injection Team[++]

LOCAL ENERGY AND PARTICLE TRANSPORT IN BURST-FREE H-PHASES OF ASDEX

ABSTRACT. Flux-surface-averaged transport in high-confinement (H) discharges with burst-free phases is analyzed by computer modelling. The electron heat diffusivity χ_e and diffusion coefficient D in undisturbed H phases are found to be about twice as small as those in ordinary H discharges with high-frequency bursts. Scaling relations for χ_e, D and ν_{in} are successfully applied. The confinement properties of ohmically heated plasmas are not recovered in the H regime. Ion heat conduction continues to be neoclassical. The steep rise of the impurity radiation loss is explained by the increase in electron density and accumulation of the iron impurity. The dominant loss channels are electron heat conduction and impurity radiation. Conductive and convective energy losses due to the ions are negligibly small.

[+] K. Bernhardi, A. Eberhagen, G. Fussmann, O. Gehre, J. Gernhardt, G.v.Gierke, E. Glock, O. Gruber, G. Haas, F. Karger, M. Keilhacker, S. Kissel, O. Klüber, M. Kornherr, K. Lackner, G. Lisitano, H.M. Mayer K. McCormick, D. Meisel, E.R. Müller, H. Murmann, W. Poschenrieder, H. Rapp, H. Röhr, F. Schneider, G. Siller, P. Smeulders, F. Söldner, K.-H. Steuer, F. Wagner

[++] E.Speth, A. Stäbler, O. Vollmer

1. Introduction

In the H discharges of ASDEX one usually observes edge localized mode (ELM) activity which causes burst-like energy and particle losses from a zone $r_s/2 \lesssim r \lesssim r_s$, where r_s = 40 cm is the separatrix radius /1,2/. In the earlier studies of H confinement with high-frequency bursts these additional fluxes were modelled by electron heat conduction and diffusion, i.e. by time-averaged transport coefficients χ_e^H and D^H /3,4,5/. These diffusivities were found to be about twice as small as those in L discharges.

In this report the confinement of burst-free H phases in the axisymmetric double-null divertor configuration is investigated by computer modelling. All simulations are carried out with modified versions /4,6/ (BALDI10R) of the BALDUR prediction transport code /7/. The observed iron impurity and corresponding radiation loss are treated with a coronal model. The rate of impurity production at the walls is calculated from sputtering due to CX neutrals.

In Sec. 2 fux-surface-averaged transport in burst-free H phases is analyzed and discussed, and the confinement properties of deuterium and iron and the impurity radiation loss are studied. The power balance is then presented and discussed in Sec. 3. Finally, in Sec. 4 the main conclusions from these studies are summarized.

2. Local transport in burst-free H phases

This section presents results from modelling H phases with high-frequency bursts and without bursts. After the diffusivites and inward drift velocity for deuterium are evaluated, the transport of the iron impurity and the corresponding radiation losses are considered.

2.1 Transport coefficients

As an example the simulation of a double-null divertor H discharge (#9910) with plasma current I_p = 380 kA, toroidal magnetic field B_t = 2.2 T and neutral injection power P_{NI} = 2.9 MW is presented. This discharge has burst-free H phases and a moderate degree of impurity, so that it is still suitable for transport studies. Hydrogen beams are injected tangentially in the co-direction into the deuterium target plasma. The measured time developments of the plasma current I_p and line-averaged density $\bar{n}_e$, shown in Fig. 1, are

prescribed in the computations. The time of transition to the H phase is marked by t_1. The H_α-D_α intensity in the divertor shows a phase with high-frequency bursts between t_1 and t_2 and burst-free phases interrupted by three large bursts. In Fig. 2 measured profiles of the electron density and temperature in the burst-free H phase at 1.3 s are compared with the simulation (solid curves). The computed iron density profile (dotted curve) exhibits a weak increase to the edge. The time developments of the central ion temperature and $\beta_{p\perp}$ are given in Fig. 3. The electron and ion temperatures saturate, while the denstiy continues to grow. This explains the increase of β_p in the experiment and computations. The profiles of χ_e^H and D^H for $t_1 \leq t < t_2$ are obtained from the empirical scaling relation, which can be expressed by dimensionless quantities and was derived from many H discharges with high-frequency bursts /4/,

$$\chi_e^H = 9.2 \times 10^3 \; r_n^{-1/2} \; T_i^{1/2} \; [\mathrm{keV}] \; r \; B_p^{-1} \; [\mathrm{kG}] \; \mathrm{cm}^2 \; \mathrm{s}^{-1}, \qquad (1)$$

$$D^H = 0.2 \; \chi_e^H, \qquad (2)$$

with $r_n = -n/\frac{\partial n}{\partial r}$. This leads to $\chi_e^H(2/3\; r_s,\; 1.2\; s) = 2.2 \times 10^4\; \mathrm{cm}^2\; \mathrm{s}^{-1}$ and $D^H(2/3\; r_s,\; 1.2\; s) = 4.4 \times 10^3\; \mathrm{cm}^2\; \mathrm{s}^{-1}$. For the inward drift velocity the empirical scaling /4/

$$v_{in} = -0.54 \; D \; (\frac{r_s}{2}) \; T_e^{-1} \; \frac{\partial T_e}{\partial r} \; \mathrm{cm}\; \mathrm{s}^{-1} \qquad (3)$$

is applicable in all phases. It yields simulations as good as those obtained by prescribing $v_{in} = 300\; (r/r_w)^2\; \mathrm{cm}\; \mathrm{s}^{-1}$ with wall radius $r_w = 49$ cm during the H phase.

For the burst-free H phase the numerical factor in Eq. (1) has to be reduced to 4.9×10^3, yielding $\chi_{e*}^H(2/3\; r_s,\; 1.3\; s) = 1.0 \times 10^4\; \mathrm{cm}^2\; \mathrm{s}^{-1}$ and $D_*^H(2/3\; r_s,\; 1.3\; s) = 2 \times 10^3\; \mathrm{cm}^2\; \mathrm{s}^{-1}$. The approximate ratio of the local coefficients $\chi_e^L : \chi_e^H : \chi_{e*}^H \approx 4 : 2 : 1$ reflects the ratio of global energy confinement times at $r = r_s$, namely $\tau_E^L \approx 30$ ms, $\tau_E^H\,(1.2\; s) \simeq 65$ ms and $\tau_{E*}^H(1.3\; s) \simeq 120$ ms. Here τ_E is defined as the thermal energy content in the plasma divided by the conductive and convective energy fluxes due to electrons and ions ($\tau_E = E_{th}/(P_e+P_i)$). It should be mentioned that $\chi_{e*}^H(r,\; 1.3\; s)$ exceeds the values derived from the OH scaling /4/ $\chi_e^{OH} = 2.5 \times 10^{17}\; n_e^{-1}\; T_{e,keV}^{-1}\; q^{-1}\; \mathrm{cm}^2\; \mathrm{s}^{-1}$ by a factor of about three. As in the ohmic and L discharges the ion heat diffusivity χ_i is 1 time the neoclassical value /8/ in both types of H phases.

Qualitatively, the confinement behaviour in the unperturbed H phases does not differ from that with high-frequency bursts discussed in the earlier papers /3,4,5/. In the H regimes with and without bursts the scaling of ohmically heated plasmas is not recovered.

2.2 The role of impurities

On the time scale of the injection period (200 ms) the influence of impurities was found to be negligibly small both in L discharges and in H discharges with high-frequency bursts. The situation changes in undisturbed H phases, where significant radiation losses due to impurities, primarily iron, are observed, which can impair the determination of the confinement properties of the plasma.

There are two obvious reasons for a faster increase of the impurity level. One is improved particle confinement in burst-free H phases which also holds for the impurities. The other reason is the larger influx of impurities from the walls due to enhanced sputtering by more energetic charge-exchange neutrals. These are produced by the higher ion temperatures in the outer plasma, which result from the better energy confinement. Moreover, the particle flux $\parallel \vec{B}$ to the divertor chambers seems to be reduced in burst-free H phases, which means that the parallel flow velocity of the deuterium plasma and the screening efficiency should be markedly less. This leads to a higher impurity influx into the main plasma even for a fixed production rate.

A coronal model which includes anomalous diffusion and inward drift is applied in order to describe the confinement of the iron impurity and the radiation losses. It is found that the diffusivities and inward drift velocities of deuterium plasmas, i.e. the scaling relations given in Eqs. (2) and (3) with the different numerical factors in the various regimes, can be applied for the iron impurity, too. They yield rather good agreement with $\beta_{p\perp}(t)$ (see Fig. 3), the bolometrically measured power in the main chamber (see Fig. 4) and the power density profile. The remaining differences between the measured and computed curves for $P_{cx} + P_{rad}$ in Fig. 4 are ascribed to variation of the impurity influx rates due to a time-dependent screening efficiency in the scrape-off plasma which is not included in the computations. According to our simulations the CX loss from the thermal plasma contributes about 300 to 450 kW. It is found that the steep rise of the power radiated by the impurity is due both to the increase in electron density and to the accumulation of iron.

In the course of the discharge the total number of iron particles within the separatrix (N_{Fe}) grows faster than the total number of electrons (N_e) reaching $N_{Fe}/N_e \simeq 1.8 \times 10^{-3}$ at 1.3 s. The corresponding Z_{eff} value in the centre amounts to 1.7.

It is worth while to note that simulations with a non-coronal model /9/ for the iron impurity yielded results nearly identical to those of the coronal calculations.

Simulations with higher iron influx rates over the separatrix were carried out for the same confinement properties and impurity production rates as in the analyzed discharge. Reducing the impurity loss rate due to parallel flow in the scrape-off zone by a factor of 5 yields $N_{Fe}/N_e \approx 10^{-2}$ and $Z_{eff}(r=0) = 4.5$ at 1.3 s. The heating power input is exceeded by the iron radiation loss, which reaches about 3 MW. Similar results were obtained experimentally in many burst-free H discharges with large impurity content.

3. Power balance

Electron heat conduction is reported to be the dominant loss channel in ASDEX L discharges and in H discharges with high-frequency bursts /3-6/. It was shown in Sec. 2.2 that in discharges with undisturbed H phases the impurity concentrations and electron density grow to a level where the radiation loss significantly contributes to the power balance.

In the H discharge under investigation the dominant loss channels at $r = r_s$ and during the burst-free phase at 1.3 s are found to be electron heat conduction (1.1 MW) and radiation (see Fig. 5). There are no indications here of an insulating sheath near the separatrix which leads to blocking of the heat flux. In this case the electron temperature profile should be much flatter than measured (see Fig. 2). The bolometrically measured power lost to the walls of the main chamber amounts to 1.1 MW (see also Fig. 4). The simulation shows that the impurity radiation and charge-exchange flux contribute 790 and 330 kW, respectively. As in the other phases the losses due to ion heat conduction (50 kW) and ion convection (100 kW) are negligibly small. The obvious difference (270 kW) between the total heating power and the sum of the power losses in Fig. 5 represents the rate of increasing the plasma energy.

The computed thermal energy contents of electrons and ions at 1.3 s are 72 and 87 kJ, respectively, and the total conductive and convective losses amount to 1.32 MW. With the above definition of the energy confinement time one thus obtains $\tau_{E*}(r_s, 1.3\ s) = 120$ ms. The corresponding volume-averaged β_t amounts to 0.8 %.

4. Conclusions

Flux-surface-averaged transport in burst-free H phases was investigated by computer modelling. A discharge with a moderate iron impurity content is chosen, since it is expected to yield the most reliable transport coefficients.

The diffusivities χ_{e*}^{H} and D_*^{H} are found to be about twice as small as those in ordinary H discharges, where additional energy and particle losses are caused by high-frequency bursts. Other differences in the confinement behaviour of H phases with and without bursts are not found. It turns out that the scaling relations for χ_e and D work with both types of H phases, if different numerical factors are applied. The confinement properties of ohmically heated plasmas are not recovered in the H regime. The ion heat diffusivity χ_i continues to be neoclassical.

It is found that the χ_e, D and v_{in} of deuterium plasmas are also approximately valid for the iron impurity. The steep rise of the power lost by impurity radiation can be explained by the increase in electron density and the accumulation of iron. Coronal and non-coronal models yield nearly identical results. The computed iron content of about 2×10^{-3} agrees with spectroscopic measurements on similar discharges.

In the burst-free H phase the dominant loss channels at the end of the injection period are electron heat conduction and impurity radiation. The discharge studied contradicts the concept of an insulating sheath near the separatrix, since blocking of the electron heat flux and rectangular T_e profiles are not found. As in the other phases, the conductive and convective energy losses due to the ions are negligibly small.

References

/1/ Wagner, F., Becker, G., Behringer, K., Campbell, D., Eberhagen, A., et al., Phys. Rev. Lett. 49 (1982) 1408.

/2/ Keilhacker, M., Becker, G., Bernhardi, K., Eberhagen, A., ElShaer, M., et al., Plasma Physics and Contr. Fusion 26 (1984) 49.

/3/ Becker, G., Campbell, D., Eberhagen, A., Gehre, O., Gernhardt, J., et al., Nuclear Fusion 23 (1983) 1293.

/4/ Becker, G., ASDEX Team and Neutral Injection Team, Report IPP III/98 (1984).

/5/ Becker, G., et al., Proc. 11th Europ. Conf. on Contr. Fusion and Plasma Physics, Aachen 1983, Vol. II, p. 299.

/6/ Becker, G., ASDEX Team, Neutral Injection Team, Nuclear Fusion 22 (1982) 1589.

/7/ Post, D.E., Singer, C.E., McKenney, A.M., PPPL Transport Group, TFTR Physics Group, Report 33 (1981).

/8/ Chang, C.S., Hinton, F.L., Phys. Fluids 25 (1982) 1493.

/9/ Lackner, K., Behringer, K., Engelhardt, W. and Wunderlich, R., Z. f. Naturforsch. 37a (1982) 931.

Figure Captions

Fig. 1:

Plasma current I_p, line-averaged density $\bar{n}_e$ and H_α-D_α intensity in the divertor versus time.

Fig. 2:

Computed $n_e(r)$ and $T_e(r)$ (solid curves) compared with the density profile measured by HCN laser interferometry (dashed curve) and with the T_e profile from ECE diagnostic (points). The dotted curve is the computed iron density profile.

Fig. 3:

$\beta_{p\perp}$ including thermal and beam contributions and central ion temperature versus time: computed (solid curves) and from diamagnetic loop (dashed curve) and CX diagnostic (points).

Fig. 4:

Time behaviour of power losses in the main chamber due to radiation P_{rad} and charge exchange P_{cx}: computed (solid curves) and measured by bolometry (dashed curve).

Fig. 5:

Profile of power balance. Power losses from the plasma within radius r result from electron heat conduction and convection P_e, ion heat conduction and convection P_i, radiation P_{rad} and charge exchange of thermal plasma P_{cx}. The absorbed beam power and ohmic heating power are denoted as P_b and P_{OH}, respectively.

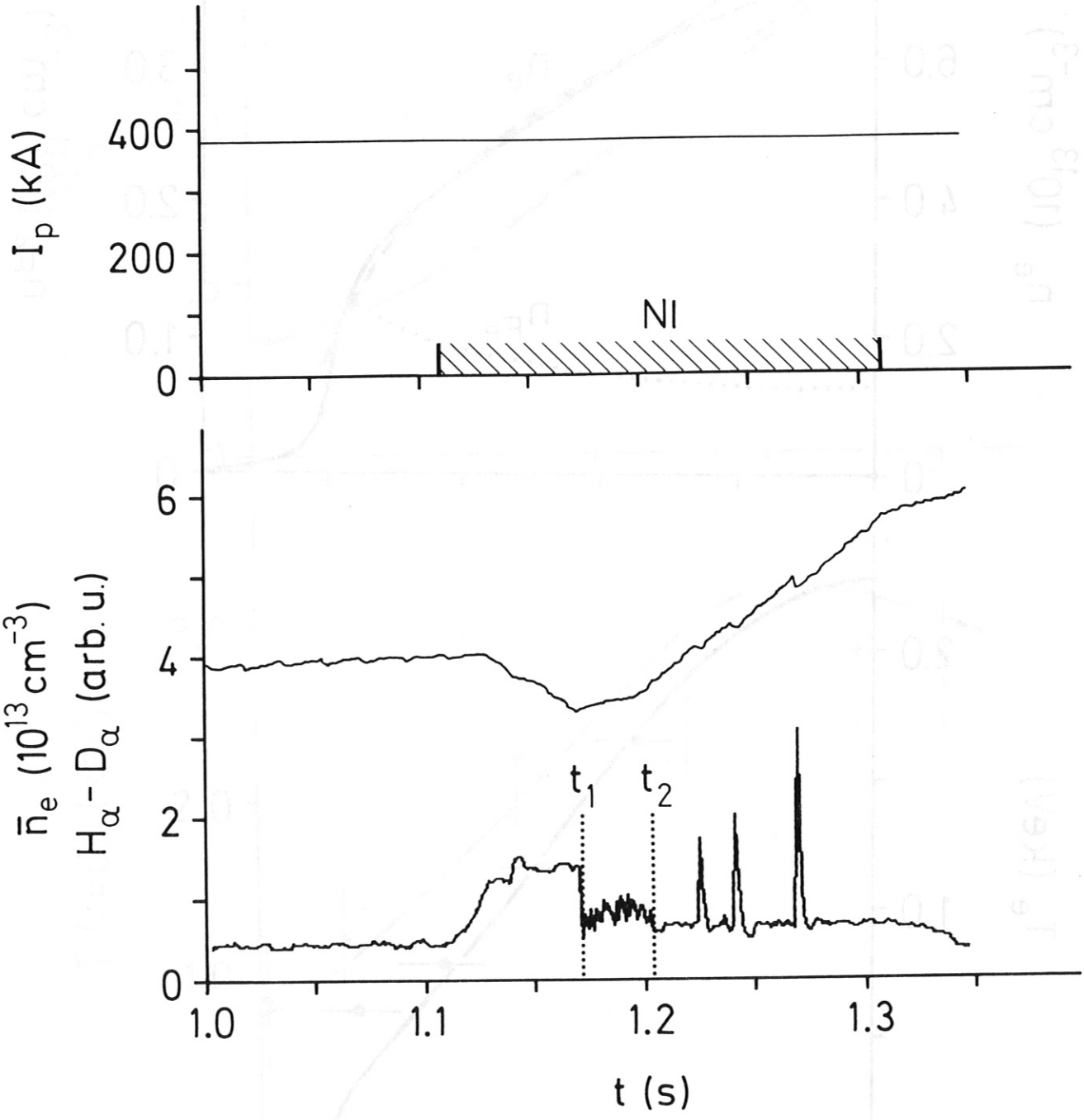
I_p (kA)
400
200
0
NI
6
4
2
0
$\bar{n}_e$ (10^{13} cm^{-3})
H_α-D_α (arb.u.)
t_1
t_2
1.0
1.1
1.2
1.3
t (s)
IPP3- BEC 326-84

Fig. 1

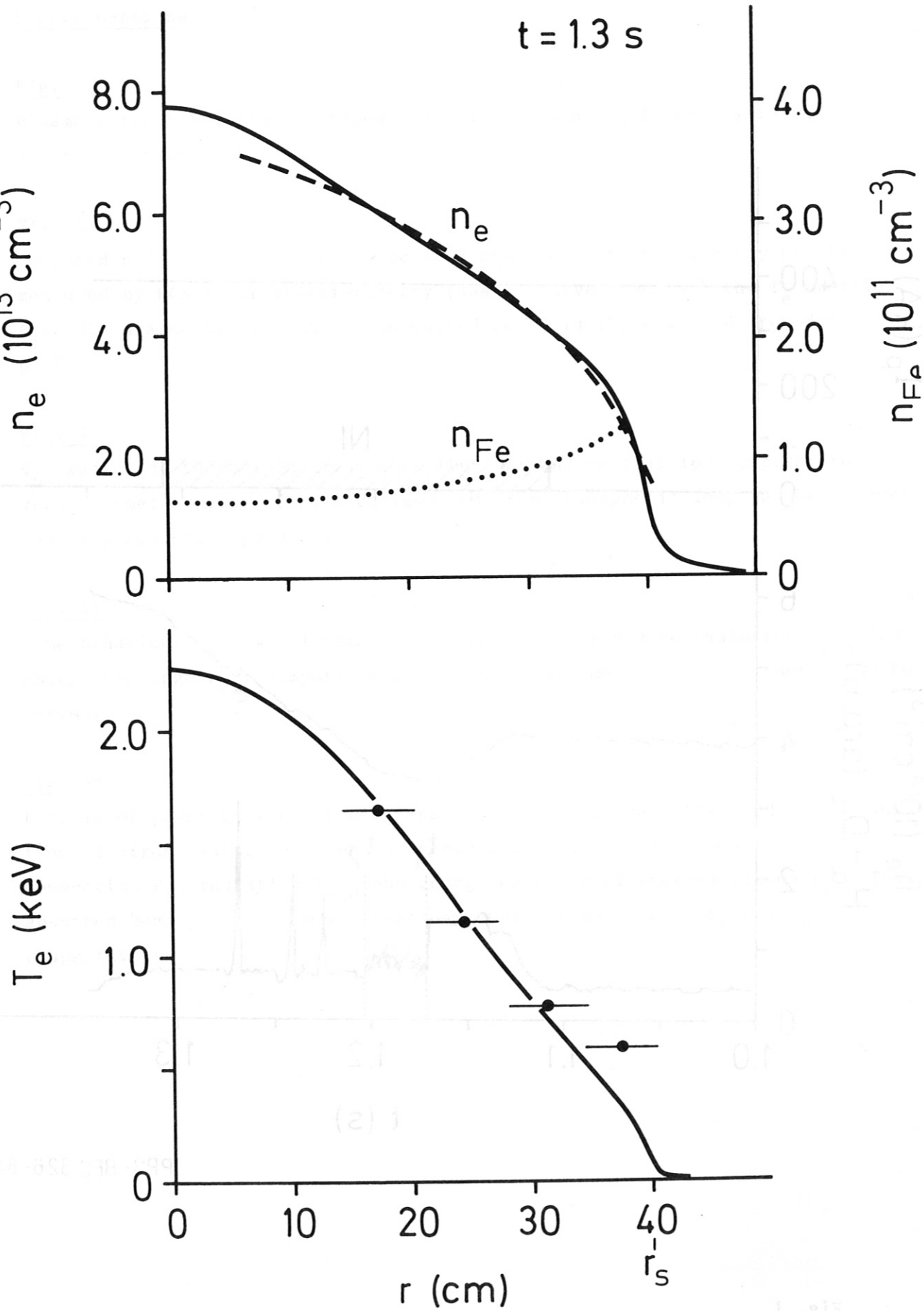

IPP3- BEC 327-84

Fig. 2

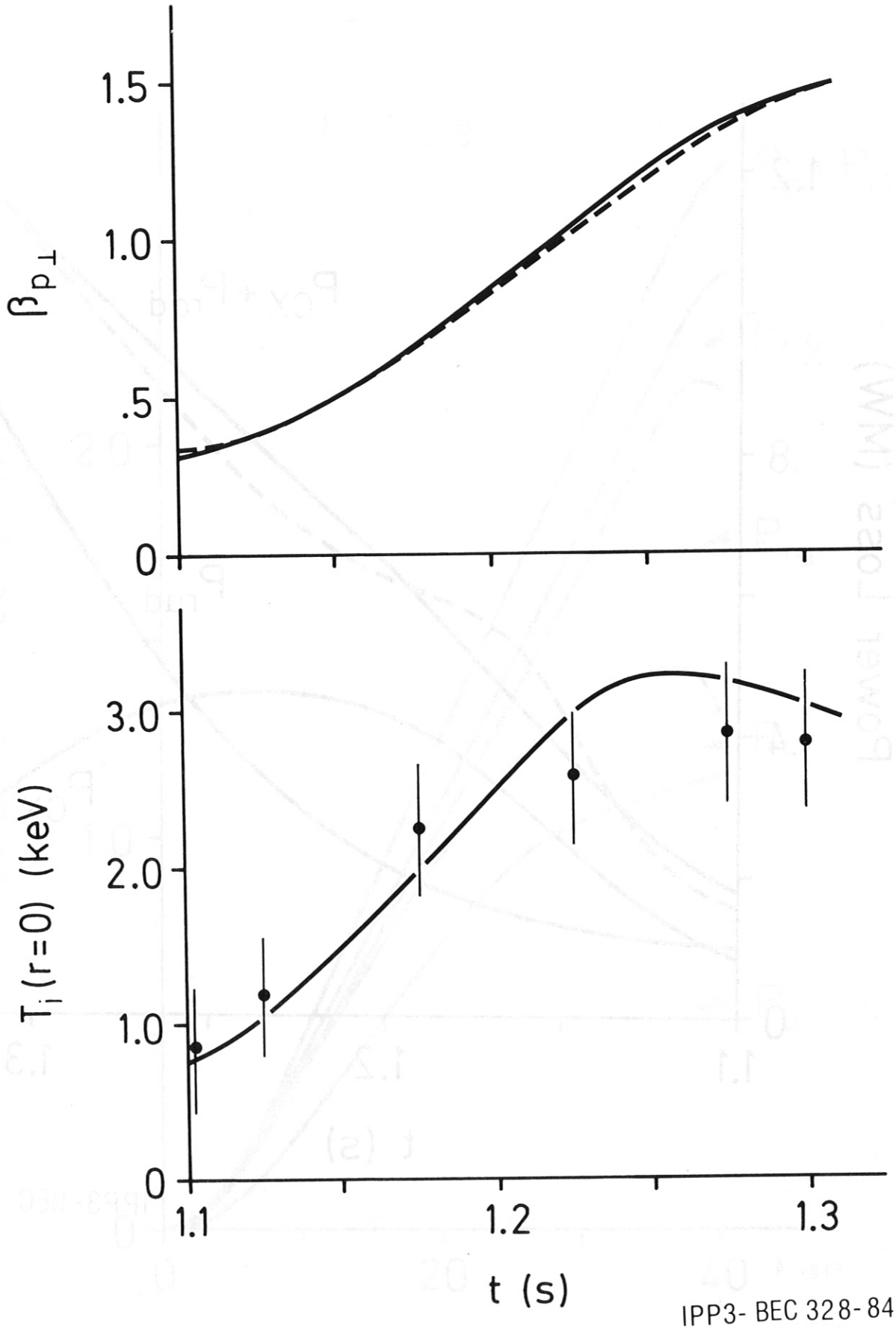

Fig. 3

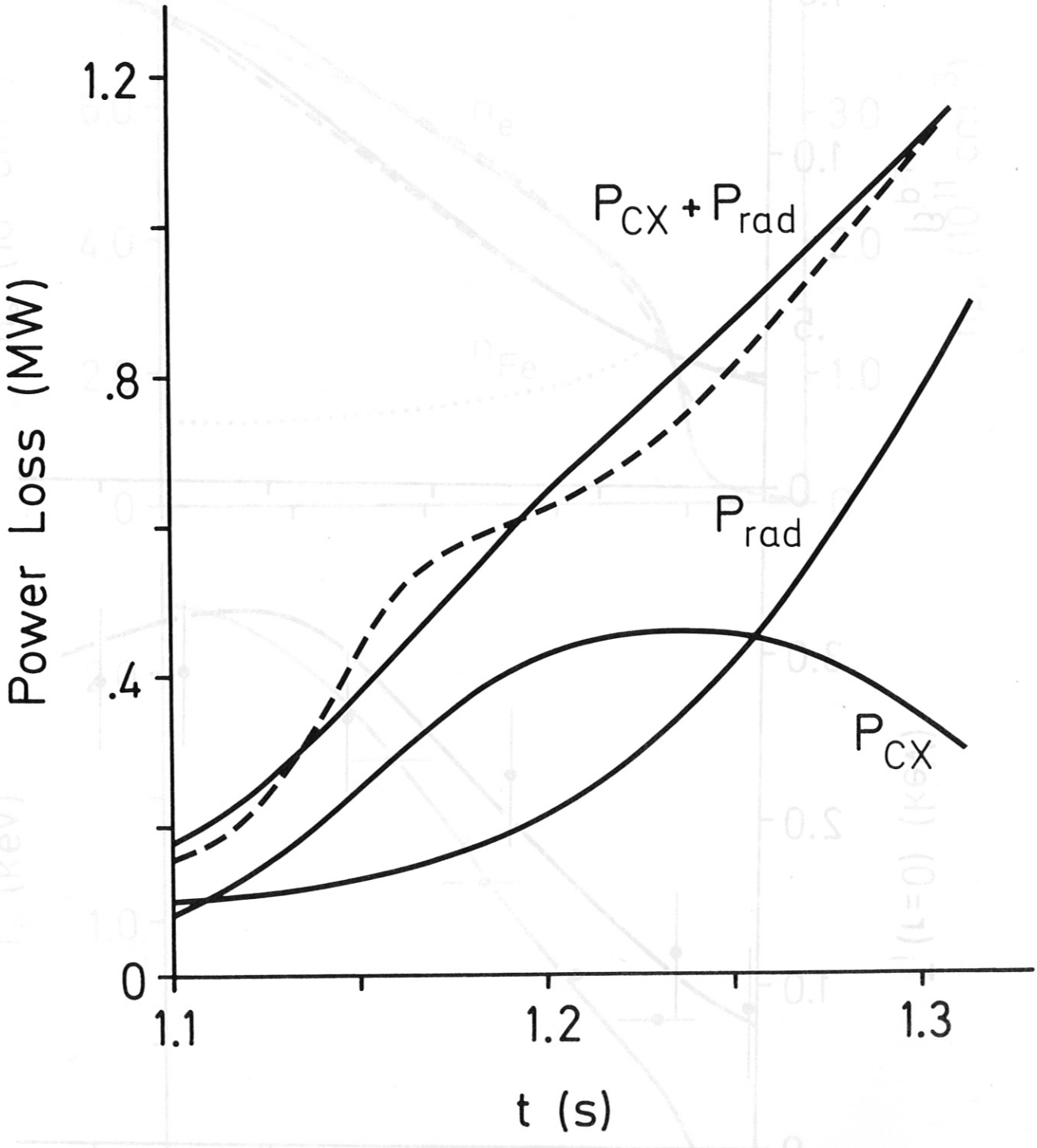

IPP3- BEC 329-84

Fig. 4

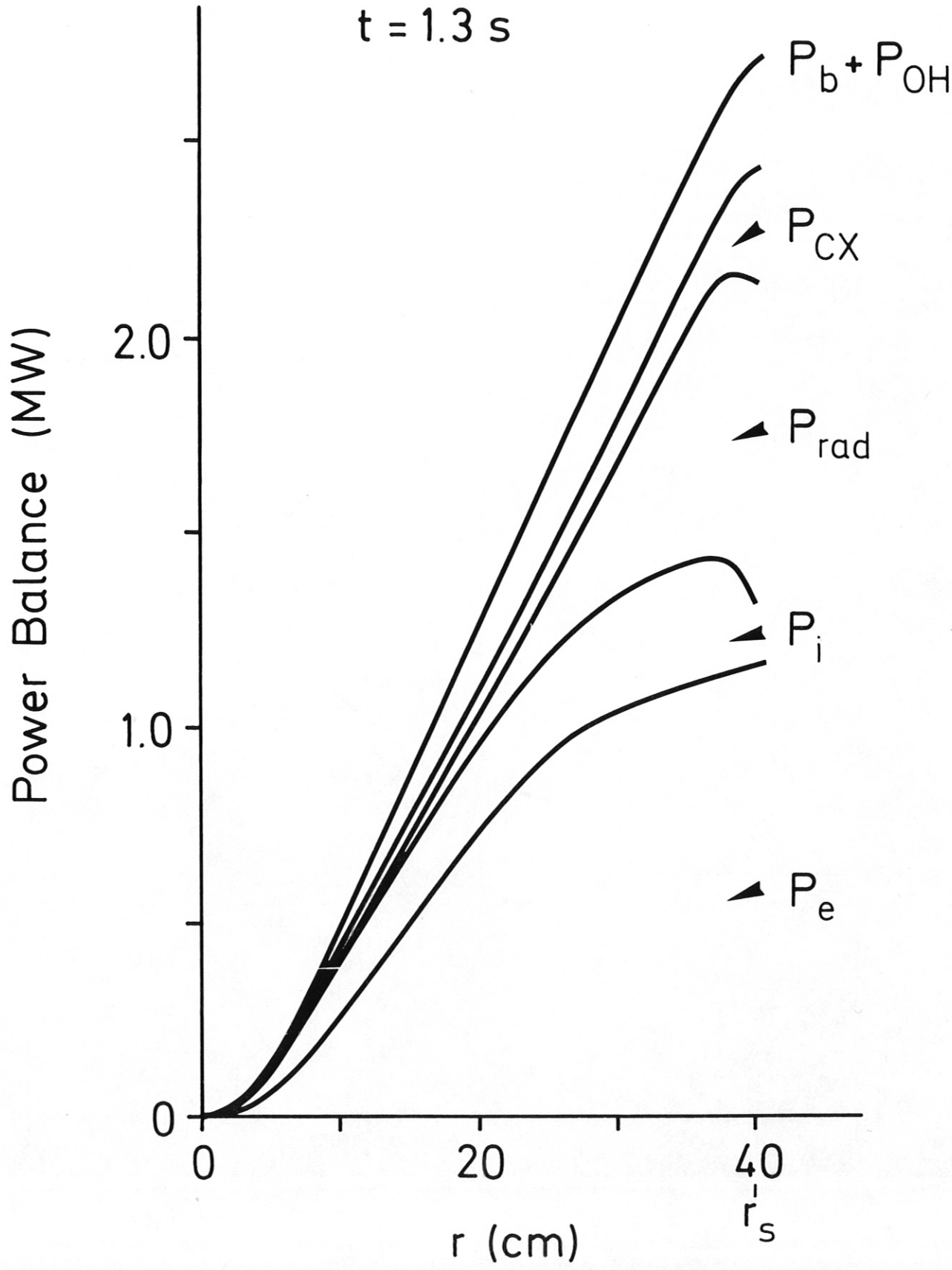

IPP3- BEC 330-84

Fig. 5